Chemical Science

ROYAL SOCIETY OF CHEMISTRY

EDGE ARTICLE

View Article Online
View Journal | View Issue

Cite this: *Chem. Sci.*, 2024, **15**, 10214

All publication charges for this article have been paid for by the Royal Society of Chemistry

Received 29th April 2024
Accepted 29th May 2024

DOI: 10.1039/d4sc02814g

rsc.li/chemical-science

Selective recognition and enrichment of C_{70} over C_{60} using an anthracene-based nanotube†

Hao Nian,‡[ab] Song-Meng Wang,‡[a] Yan-Fang Wang,[a] Yu-Tao Zheng,[a] Li-Shuo Zheng,[a] Xiaoping Wang,[a] Liu-Pan Yang, *[c] Wei Jiang §*[a] and Liping Cao *[b]

Selective recognition and enrichment of fullerenes (*e.g.*, C_{60} and C_{70}) remains challenging due to the same diameter and geometrical similarity. Herein, we report a hexagonal anthracene-based nanotube (**1**) through a one-pot Suzuki–Miyaura cross-coupling reaction. With anthracene-based side walls and pyridine linkers, **1** features a nano-scale tubular cavity measuring 1.2 nm in diameter and 0.9 nm in depth, along with pH-responsive properties. Interestingly, the electron-rich **1** shows high binding affinity ($K_a \approx 10^6$ M^{-1}) and selectivity ($K_s \approx 140$) to C_{70} over C_{60} in toluene, resulting from their different contribution of π–π interactions with the host. The protonation of **1** simultaneously alters the electronic properties within the nanotube, resulting in the release of the fullerene guests. Lastly, the selective recognition and pH stimuli-responsive properties of the nanotube have been utilized to enrich C_{70} from its low-content mixtures of fullerenes in chloroform.

Introduction

Since Krätschmer and coworkers reported the extraction of C_{60} and C_{70} from carbon soot by using aromatic solvents in 1990,[1] a number of artificial receptors have been extensively developed for the recognition and separation of fullerenes.[2,3] Most traditional macrocyclic hosts and their derivatives, such as γ-cyclodextrin (γ-CD),[4–7] calix[*n*]arenes,[8–13] pillar[10]arene,[14] and theoretical cucurbit[9]uril (CB[9]),[15] have shown similar binding affinities to fullerene compounds including C_{60} and C_{70}. There are still many challenges in efficiently distinguishing C_{60} and C_{70} through molecular recognition. For example, C_{60} and C_{70} have the same diameter but differ in length, leading to challenges in their selective recognition. This requirement implies that there is variation in the geometric-shape matching between the receptors' cavities and different fullerenes. On the other hand, fullerenes can be regarded as electron-deficient guests in the host–guest interaction. The electron-rich aromatic units, such as porphyrins,[16–18] anthracene,[19,20] and nanographene[21] can be used as building blocks to achieve the complementary charge interactions with fullerenes. As a result, several fullerene-selective receptors with various geometric-shape cavities have been reported (Scheme 1a), including molecular cages,[22] coordination capsules,[23] deep cavitands,[24] and so on. These three-dimensional (3D) structures with both restricted cavities and buried π–π interactions have achieved selective binding for fullerenes based on the shape matching and/or the charge complementation.

The design and synthesis of macrocyclic compounds has been one of the interesting areas for supramolecular chemists.[25,26] Especially, a class of aromatic macrocycles with nano-scale cavities, such as cycloparaphenylenes (CPPs)[27–29] and cyclophanes,[30–32] can bind to the outer convex surface of a fullerene within their inner concave surfaces *via* the charge- and shape-complementary π–π interactions. However, the selective recognition of fullerenes by aromatic macrocycles or nanotubes has been rarely achieved. Although there are some examples, the selectivity of fullerenes is still not satisfactory for their separation.[33,34] In fact, there are enormous challenges associated with selective recognition of macrocyclic hosts for fullerenes, including issues related to synthesis procedures, molecular structure design, and control over flexibility for size expansion. In general, large macrocycles that are tailored to the size of fullerenes can be synthesized by increasing both the number[14] and size[35,36] of building blocks.[37,38] However, the flexibility may increase with the enlargement of the ring size, which may cause the collapse of the macrocyclic compounds.[39] Additionally, a more intricate molecular structure is required to differentiate the small size disparity between C_{60} and C_{70} (Scheme 1b). Therefore, an effective solution is to achieve selective recognition by matching the size of a macrocyclic cavity with different fullerenes.

[a]*Department of Chemistry, Southern University of Science and Technology, Xueyuan Blvd 1088, Shenzhen, 518055, China. E-mail: jiangw@sustech.edu.cn*

[b]*College of Chemistry and Materials Science, Northwest University, Xi'an, 710069, P. R. China. E-mail: chcaoliping@nwu.edu.cn*

[c]*School of Pharmaceutical Science, University of South China, Hengyang, Hunan, 421001, China. E-mail: yanglp@usc.edu.cn*

† Electronic supplementary information (ESI) available. CCDC 2323307. For ESI and crystallographic data in CIF or other electronic format see DOI: https://doi.org/10.1039/d4sc02814g

‡ These authors contributed equally to this work.

§ Deceased (2022.12).

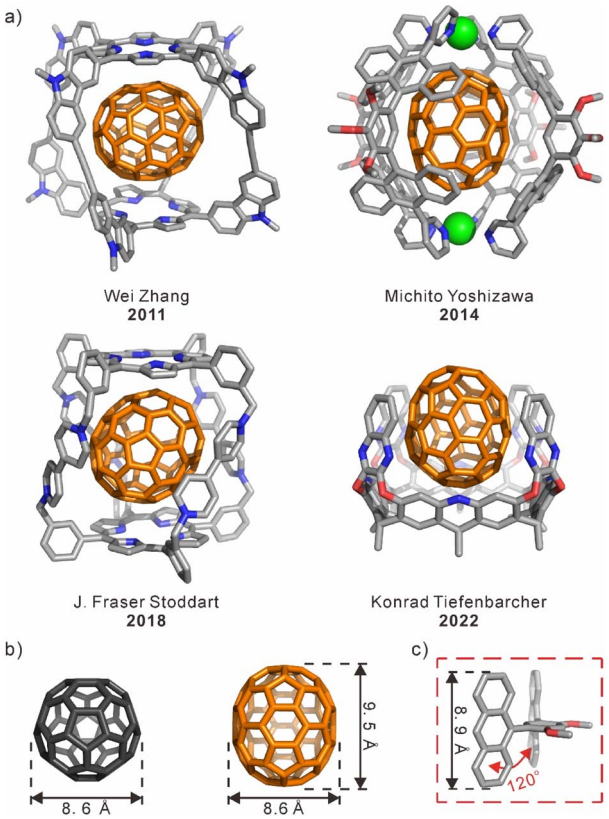

Scheme 1 (a) Representative samples of the host⊃C_{70} complexes. (b) Comparison of the sizes of C_{60} and C_{70}. (c) The bent structure of the anthracene-dimer building block.

The anthracene-dimer building block[19,40] with a bent structure of 120° angle was used to construct a series of coordination capsules/tubes,[23] covalent nanotubes,[41] and polyaromatic capsules (Scheme 1c).[42,43] And, anthracene, as a large aromatic electron-rich panel with a length comparable to that of C_{70}, could be a suitable building block for constructing receptors to selectively recognize C_{70} over C_{60}.[42,44] Herein, we have designed and synthesized a hexagonal anthracene-based nanotube (**1**) formed from three anthracene-dimer building blocks and three 2,6-dibromo-4-methoxypyridine rings *via* a one-pot Suzuki–Miyaura cross-coupling reaction. In the macrocyclic structure of **1**, six anthracene panels serve as side walls and are covalently linked through alternating benzene and pyridine rings to form a hexagonal cavity. Interestingly, the size of the inner cavity with the diameter of ~1.2 nm and the depth of ~0.9 nm perfectly matches with the size of C_{70}. As a result, the nanotube can selectively encapsulate C_{70} along the long axis *via* enhanced π–π interactions over C_{60}, showing a high binding selectivity (K_s) of ~140 times. On the other hand, the pH stimuli-responsive properties of the nanotube were verified through NMR, UV-vis, and fluorescence spectroscopy, which are attributed to the protonation and deprotonation of the pyridine rings in the nanotube. As a result, this anthracene-based nanotube was successfully employed in the enrichment of C_{70} from a fullerene mixture enriched with C_{60}, owing to its selectivity towards C_{70} and pH stimuli-responsive properties.

Results and discussion

The synthetic route of the nanotube is shown in Fig. 1a. First, $\mathbf{2_{Bpin}}$ can be directly obtained by $\mathbf{2_{Br}}$ through the Miyaura borylation reaction (Fig. S1–S4†). The anthracene-based nanotube

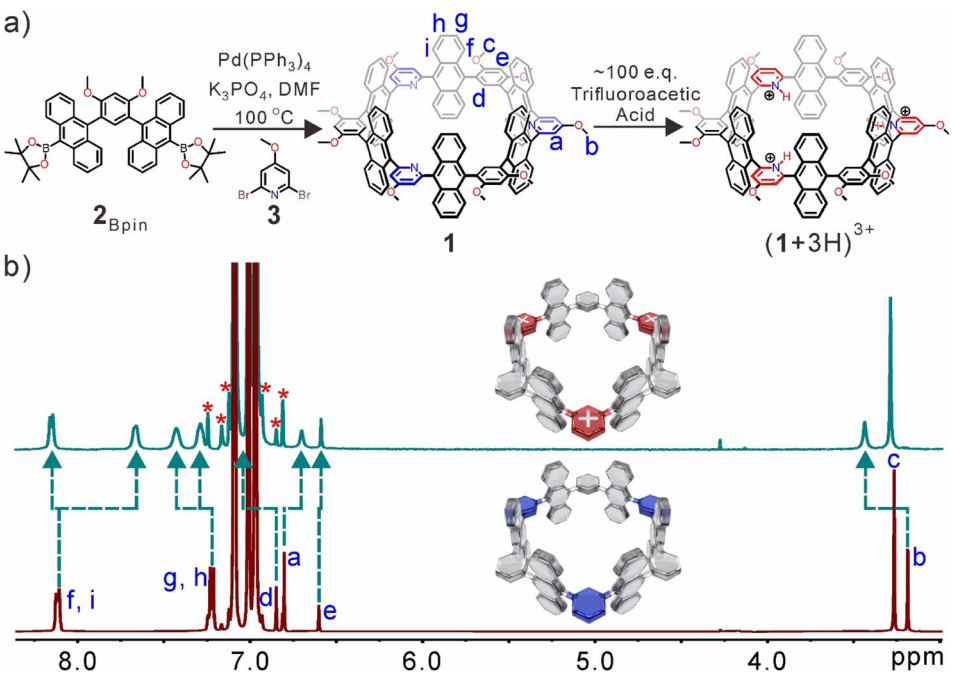

Fig. 1 (a) Synthesis of **1** and its protonation. (b) Partial ^{1}H NMR spectra of **1** (bottom) and $(\mathbf{1} + 3H)^{3+}$ (top) in toluene-d_8 at 298 K. The satellite peaks of solvents are indicated by the asterisk symbol.

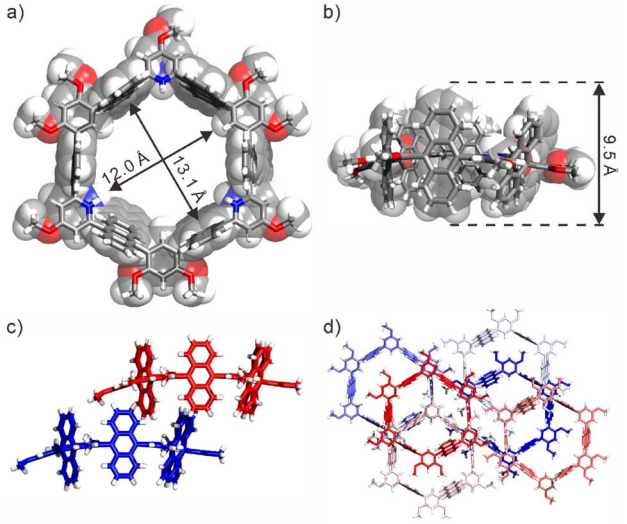

Fig. 2 X-ray structures of $(\mathbf{1} + 3H)^{3+}(TFA^{-})_3$: (a) top view and (b) side view of a single molecule; (c) side view of neighboring nanotubes inserted into each other; (d) top view of the structure of the packing nanotubes. For clarity, all counterions and solvent molecules are omitted. CCDC No.: 2323307.

1·was synthesized in ~5% yield from a one-pot Suzuki–Miyaura cross-coupling of $\mathbf{2_{Bpin}}$ and 2,6-dibromo-4-methoxypyridine (**3**) in a 1 : 1 molar ratio (Fig. S5†). **1** was fully characterized by ^{1}H, ^{13}C, and 2D NMR spectroscopy as well as high-resolution mass spectrometry (HR-MS) measurements (Fig. S6–S10†). The nanotube displayed good solubility in toluene, chloroform, and dichloromethane, but was insoluble in methanol. A highly symmetric structure was indicated by ^{1}H NMR spectra, and no significant aggregation or other conformational isomers were observed at NMR concentrations (Fig. S6†). Notably, the inward-directed nitrogen atoms of pyridine rings can be protonated by adding excess trifluoroacetic acid (TFA) (Fig. 1b). The simplicity of the NMR signals suggested that all pyridine rings were protonated, and significant splitting of anthracene rings was observed (H_{f-i}), which indicated that anthracene rings were situated in a more asymmetric chemical environment. The electron cloud density of pyridine rings decreased after full protonation, resulting in the proton resonances of anthracene (H_i) and pyridine (H_a) groups displayed obvious upfield shifts because these protons are located at the deshielding area of pyridine rings. However, the other proton resonances (H_b, H_d, and H_{g-h}) were significantly shifted downfield. There are little shifts of protons H_c and H_e on the benzene rings, due to a more positive electronic environment of the inner cavity. The broad peaks implied that the solubility of the protonated nanotube in toluene-d_8 was slightly reduced under the acidic conditions.

Fluorescence experiments were conducted to investigate the pH stimuli-responsive properties of **1**. The unprotonated **1** exhibited a distinct anthracene monomer emission at 436 nm

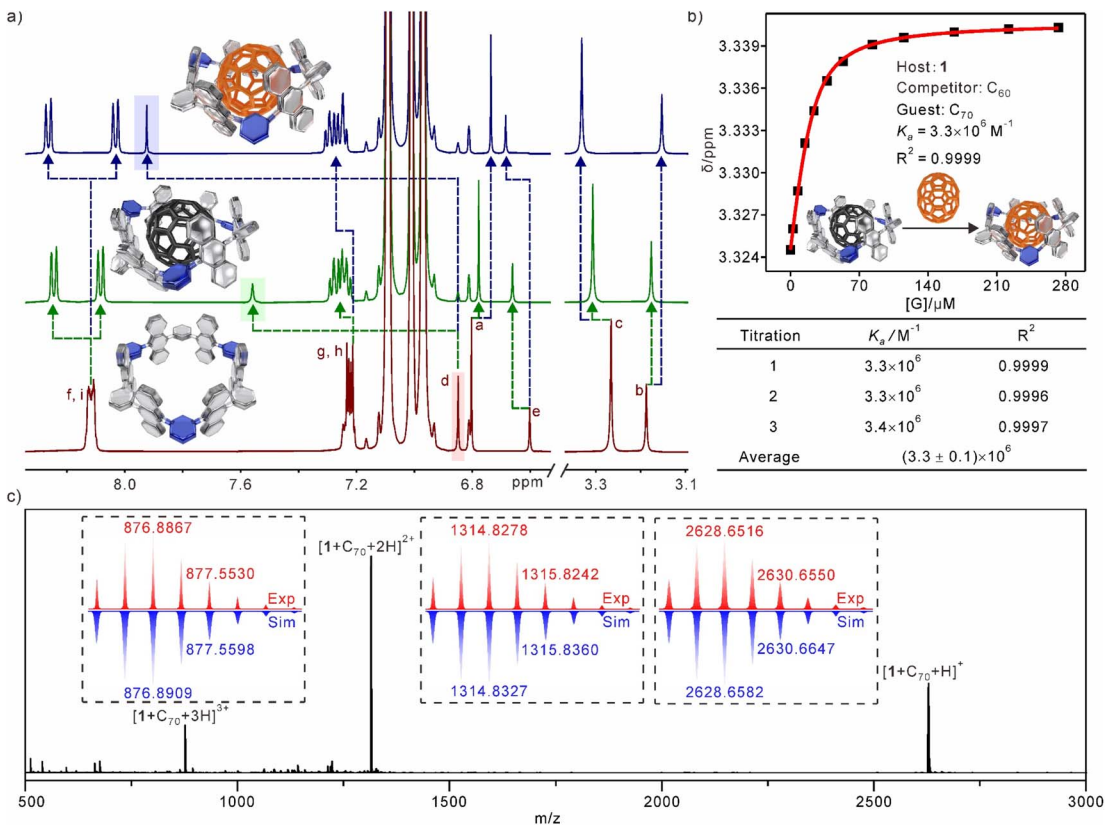

Fig. 3 (a) Partial ^{1}H NMR spectra (500 MHz, toluene-d_8, 298 K) recorded for (bottom) **1**, (medium) **1** ⊃ C_{60}, and (top) **1** ⊃ C_{70} ([**1**] = 2.0 mM; [C_{60} and C_{70}] = 2.0 mM); (b) competitive ^{1}H NMR experiment and association constant of **1** ⊃ C_{70}; (c) experimental and simulated ESI mass spectra of **1** ⊃ C_{70}.

(Fig. S11a†). Upon gradual addition of TFA, the monomer emission decreased while the anthracene excimer emission at ~518 nm increased progressively, indicating the formation of the protonated nanotube. As anticipated, the protonated nanotube could be neutralized by the addition of triethylamine (TEA), resulting in a blueshift from excimer to monomer emission after excessive TEA addition (Fig. S11b†). The reversible response of the nanotube to pH was supported by the UV-vis absorption spectra (Fig. S11c†). Furthermore, dilution of the protonated nanotube led to an increase in excimer emission (Fig. S11d†), followed by a gradual blueshift. These findings highlight the pH stimuli-responsive nature and intriguing photophysical properties of the nanotube, which will be utilized for the release of guests. Fortunately, single crystals of the protonated nanotube suitable for X-ray measurement were obtained by adding an appropriate amount of trifluoroacetic acid (TFA) to a solution of **1** in toluene because the protonated nanotube has lower solubility (Fig. 2, S12 and Table S2†). In the X-ray structure of $(\mathbf{1}+3H)^{3+}\cdot(TFA^{-})_3$, six anthracene rings, three benzene rings, and three protonated pyridine rings mainly formed the hexagonal nanotube with a diameter above 1.2 nm (Fig. 2a). Among them, six anthracene rings are perpendicular to the equatorial plane of the nanotube, while the benzene rings and protonated pyridine rings are parallel to the equatorial plane of the nanotube, forming a tubular cavity with a depth of ~0.9 nm (Fig. 2b). Furthermore, adjacent nanotubes were inserted into each other, where the cavities of the nanotubes or the gaps between the nanotubes are filled with TFA^{-} and toluene molecules (Fig. 2c). This insertion was accompanied by a slight curvature of the equatorial plane, leading to the blockage of the pore structure of the nanotubes (Fig. 2d).

Based on the X-ray structure, the diameter size of the inner cavity of the nanotube is well matched with the size of the fullerenes. Initially, the 1 : 1 host–guest complexes formed from **1** and fullerenes (including C_{60} and C_{70}) were investigated using ^{1}H NMR spectra (Fig. 3a). Fullerenes can be considered as electron acceptors. Consequently, the addition of fullerenes to nanotubes results in a significant chemical shift of the proton H_d, which is directed towards the inner part of the cavity. The π–π interactions between fullerenes and nanotubes greatly diminish the shielding effects of the anthracene rings. As a result, the proton H_d, which is located within the shielding area in the complex, experienced a significant downfield shift. Additionally, the CH···π interactions between H_d and fullerenes also play a role in the observed downfield shift. Similarly, the resonances of the methoxy proton (H_c) and the proton (H_e) on the benzene rings exhibit slight downfield shifts. The protons of the anthracene rings exhibit distinct splitting patterns. Specifically, H_i and H_f split into two separate sets of peaks, while H_g and H_h, which are located at the port of the nanotube, experience only a slight split. These findings suggest that the fullerenes are completely encapsulated within the cavity and primarily bind to the equatorial plane of the nanotube. The electron-deficient nature of the pyridine ring leads to a significant upfield shift of the protons $H_{a,b}$ in the presence of the fullerene ring current in complexes. The chemical shifts of **1** ⊃ C_{70} were observed to be more significant compared to those of **1** ⊃ C_{60}, suggesting a stronger interaction between **1** and C_{70} than with C_{60}. To determine the affinities of nanotubes to fullerenes, ^{1}H NMR titration experiments were used to calculate the association constants (K_a) of the host–guest complexes. The K_a of **1** ⊃ C_{60} could be measured to be 2.3×10^4 M^{-1} by using the 1 : 1 binding mode in toluene-d_8 (Fig. S13†). The competitive ^{1}H NMR experiment confirmed a higher binding affinity for **1** ⊃ C_{70} ($K_a = 3.3 \times 10^6$ M^{-1}), in which C_{60} was used as a competitor (Fig. 3b and S14†). Fluorescence titration experiments (Fig. S15 and S16†) were employed to further confirm the association constants ($K_a = 3.3 \times 10^4$ M^{-1} and 3.1×10^6 M^{-1} for **1** ⊃ C_{60} and **1** ⊃ C_{70}, respectively), which were consistent with the results from ^{1}H NMR titration experiments. Job plots and HR-MS strongly supported the 1 : 1 binding stoichiometry between **1** and fullerenes (Fig. 3c, and S17–S19†). The results of all host–guest experiments consistently indicated that the nanotube cavity is sufficiently spacious to fully encapsulate the entire fullerene molecules.

Despite the similarities in structure and properties among fullerenes, the nanotube demonstrated a remarkable binding selectivity ($K_s \approx 140$) between C_{70} and C_{60}. To gain deep insights into the selectivity of **1** for fullerenes, theoretical calculations

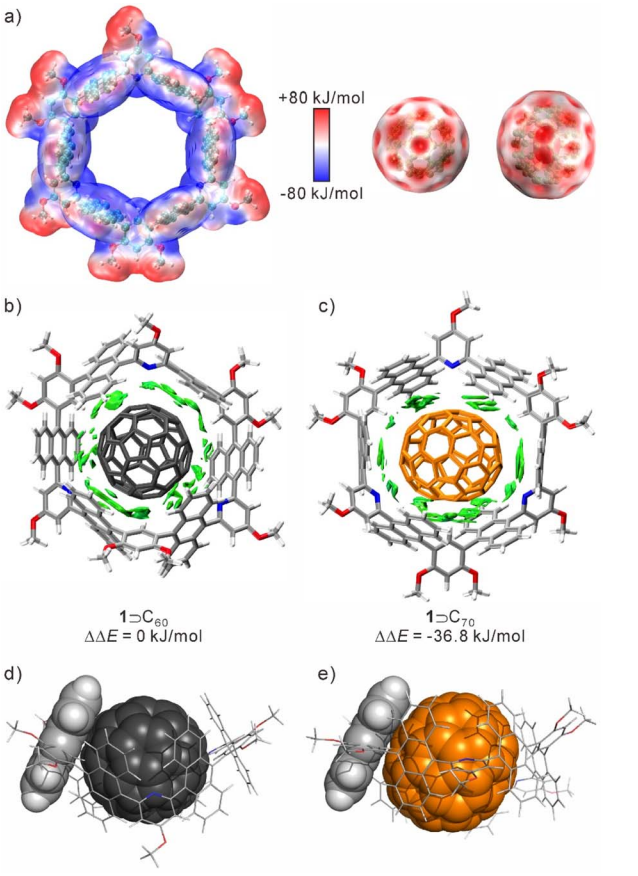

Fig. 4 (a) Electrostatic potential surface of **1**, C_{60}, and C_{70}; non-covalent interaction analysis (using an independent gradient model based on Hirshfeld partition, IGMH)[45] for (b) **1** ⊃ C_{70} and (c) **1** ⊃ C_{60}, using the ωB97XD functional[46] together with the Pople basis set;[47] side view of the anthracene fragment and (d) C_{60} and (e) C_{70}.

were performed using Density Functional Theory (DFT) and with the Multiwfn program to process wavefunction files.[48] As shown in Fig. 4a, the concave cavity of **1** is electron-rich and complements the electron-deficient convex surface of fullerenes. In both **1** ⊃ C_{60} and **1** ⊃ C_{70}, the shortest atom-to-atom distances between the aromatic ring and fullerenes were ≈3.1–3.3 Å. The CH···π interactions were also observed arising from benzene rings and guests, which were around 2.5 Å and 2.4 Å for **1** ⊃ C_{60} and **1** ⊃ C_{70}, respectively. In the host–guest binding structures, the anthracene planes undergo rotation along the equatorial plane of the nanotube. This conformational adaptation optimizes the π–π interactions between the anthracene fragments and fullerenes (Fig. 4b, c and S20†).

Moreover, the lengths of the anthracene planes and C_{70} are more matched, resulting in an increased contact area between the host and guest. This matching could potentially contribute to the selectivity of **1** towards C_{70} over C_{60} (Fig. 4d and e). Meanwhile, the HOMO and LUMO of the complexes were mainly located on the anthracene rings and fullerenes, and the energy gaps were 5.38 eV for **1** ⊃ C_{60} and 5.32 eV for **1** ⊃ C_{70}, respectively (Fig. S21 and S22†). By comparing the binding energy of **1** ⊃ C_{60} and **1** ⊃ C_{70}, the binding affinity of **1** ⊃ C_{70} is stronger than that of **1** ⊃ C_{60}, with a lower free energy of -36.8 kJ mol^{-1}. The selectivity is primarily driven by enthalpic differences, with a slight entropic contribution, as revealed by the analysis of thermodynamic parameters (Table S2†). This suggests that the nanotube may undergo more shape changes to achieve maximum contact with the guest during the binding process of C_{60}. Additionally, due to its longer size and larger volume, C_{70} is better suited to the volume and shape of the host cavity compared to C_{60}.

The protonation of the inward-directed pyridine rings can alter the electronic environment of the inner cavity, leading to a decrease in electron cloud density within the cavity. As a result, the binding between the nanotube and fullerenes could be dissociated under the low pH conditions. Based on the binding selectivity for fullerenes and pH stimuli-responsive properties of **1**, the separation of C_{70} from C_{60}-enriched fullerene mixtures by using **1** as extractant was explored.[17] First, the release of the fullerenes was observed by adding excess TFA through UV-vis and ^{1}H NMR experiments (Fig. S23 and S24†). In the NMR spectra, signals corresponding to complexes disappeared, and a new set of signals appeared, which corresponded to the protonated nanotube. The protonated nanotube was also subjected to theoretical calculations (Fig. S25†). The electrostatic potential surface (EPS) of the $(\mathbf{1} + 3H)^{3+}$ species exhibited a significantly higher positive charge compared to the unprotonated **1**. As a result, the EPS of the nanotube and fullerenes, which was previously in equilibrium, became repulsive. This repulsion, along with the change in the internal volume of the cavity before and after protonation, contributes to the release of fullerenes.

Next, the enrichment of C_{70} from the C_{60}/C_{70} ($n:n = 9:1$) mixture was investigated using UV-vis absorption spectra (Fig. 5). A mixture of C_{60}/C_{70} with **1** in chloroform was set as the test group, while the mixture of C_{60}/C_{70} was set without the

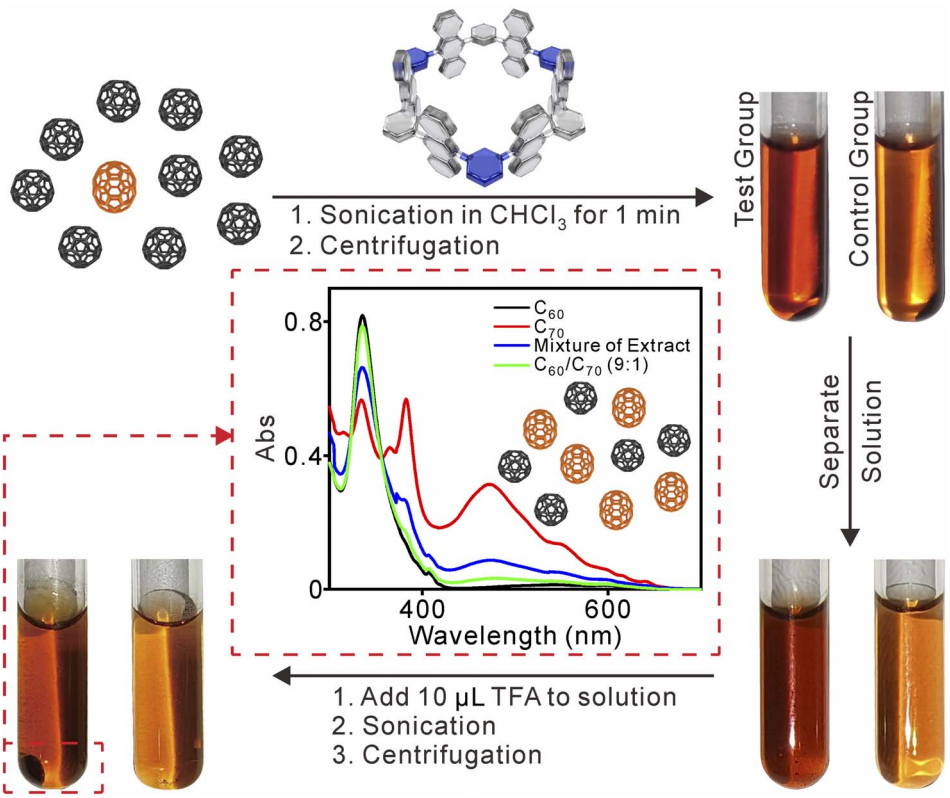

Fig. 5 Schematic presentation and UV-vis spectra of the C_{70} enrichment process.

nanotube as the control experiment. The two mixed groups were sonicated for 1 min, and the solvent was separated by centrifugation. The solution color of the test group was darker compared with the control group, indicating that **1** may increase the solubility of the fullerene by forming **1** ⊃ fullerene complexes in chloroform. After the addition of acid and sonication, a black solid precipitated in the test group, while no precipitation occurred in the control group. The solid was separated, and **1** could be regenerated by neutralization with TEA. The UV-vis absorption revealed an increase in C_{70} content from ~10% to ~50% after just one cycle.[17] This result demonstrates the selective binding and enrichment capability of **1** for C_{70} in a mixture of fullerenes.

Conclusions

In conclusion, we have developed the synthesis of an anthracene-based nanotube with a hexagonal cavity of ~1.2 nm × 0.9 nm. The selective binding and pH stimuli-responsive behaviors of the nanotube with C_{60} and C_{70} were investigated by NMR, fluorescence, UV-vis, and HR-MS experiments. The electron-rich cavity formed by anthracene-based side walls exhibited high affinity and selectivity to C_{70} over C_{60}. Theoretical calculations showed that the selectivity is primarily driven by enhanced π–π interactions between anthracene fragments and fullerenes. Moreover, this study successfully achieved the enrichment of C_{70} from its low-content mixtures of fullerenes. As a result, these findings provide significant insights into the selective recognition of fullerene molecules and contribute to the expansion of the family of supramolecular hosts with nanoscale recognition cavities.

Data availability

All data, including experimental details, computational details, characterization data, ^{1}H NMR spectra of the complexes, ^{1}H NMR titration data, UV-vis spectra, fluorescent titration data, are available in Supplementary Information.

Author contributions

W. J. conceived and designed the experiments. L. C., and L.-P. Y. supervised the research. H. N. and S.-M. W. carried out the experiments and performed the DFT calculations. Y.-F. W. solved crystal structures. L. C., L.-P. Y., H. N., S.-M. W., Y.-F. W., Y.-T. Z., L.-S. Z., and X. W. analyzed the data. H. N., S.-M. W. and L. C. wrote, reviewed and edited the manuscript with contributions from all the authors.

Conflicts of interest

There are no conflicts to declare.

Acknowledgements

We are grateful for the technical support from SUSTech-CRF and the Center for Computational Science and Engineering of SUSTech. The calculations were also performed by using the CHEM high-performance supercomputer cluster (CHEM-HPC) located at the Department of chemistry, SUSTech. L. C. acknowledges the funding support from the National Natural Science Foundation of China (22122108 and 22371229).

Notes and references

1 W. Krätschmer, L. D. Lamb, K. Fostiropoulos and D. R. Huffman, *Nature*, 1990, **347**, 354–358.
2 F. Diederich and M. Gómez-López, *Chem. Soc. Rev.*, 1999, **28**, 263–277.
3 T. Kawase, in *Supramolecular Chemistry of Fullerenes and Carbon Nanotubes*, ed. N. Martín and J.-F. Nierengarten, Wiley-VCH, Weinheim, Germany, 2012, ch. 3, pp. 55–78.
4 T. Andersson, K. Nilsson, M. Sundahl, G. Westman and O. Wennerström, *J. Chem. Soc., Chem. Commun.*, 1992, 604–606.
5 Y. Takeda, T. Nagamachi, K. Nishikori and S. Minakata, *Asian J. Org. Chem.*, 2012, **2**, 69–73.
6 A. Ikeda, M. Ishikawa, R. Aono, J. Kikuchi, M. Akiyama and W. Shinoda, *J. Org. Chem.*, 2013, **78**, 2534–2541.
7 K. Miki, Z. Dan Zhang, K. Kaneko, Y. Kakiuchi, K. Kojima, A. Enomoto, M. Oe, K. Nogita, Y. Murata, H. Harada and K. Ohe, *Mater. Adv.*, 2022, **3**, 312–317.
8 M. Yanase, T. Haino and Y. Fukazawa, *Tetrahedron Lett.*, 1999, **40**, 2781–2784.
9 T. Haino, Y. Matsumoto and Y. Fukazawa, *J. Am. Chem. Soc.*, 2005, **127**, 8936–8937.
10 S.-Q. Liu, D.-X. Wang, Q.-Y. Zheng and M.-X. Wang, *Chem. Commun.*, 2007, 3856–3858.
11 T. Haino, M. Yanase and Y. Fukazawa, *Angew. Chem., Int. Ed.*, 1998, **37**, 997–998.
12 T. Haino, C. Fukunaga and Y. Fukazawa, *Org. Lett.*, 2006, **8**, 3545–3548.
13 T. Haino, C. Fukunaga and Y. Fukazawa, *J. Nanosci. Nanotechnol.*, 2007, **7**, 1386–1388.
14 T. Ogoshi, N. Ueshima, F. Sakakibara, T. A. Yamagishi and T. Haino, *Org. Lett.*, 2014, **16**, 2896–2899.
15 G. Colherinhas, E. E. Fileti and T. Malaspina, *J. Mol. Model.*, 2018, **24**, 181.
16 P. D. W. Boyd, M. C. Hodgson, C. E. F. Rickard, A. G. Oliver, L. Chaker, P. J. Brothers, R. D. Bolskar, F. S. Tham and C. A. Reed, *J. Am. Chem. Soc.*, 1999, **121**, 10487–10495.
17 C. Zhang, Q. Wang, H. Long and W. Zhang, *J. Am. Chem. Soc.*, 2011, **133**, 20995–21001.
18 H. Liu, C. Guo, L. Li, Z. Zhang, Y. Hou, C. Mu, G.-L. Hou, Z. Zhang, H. Wang, X. Li and M. Zhang, *J. Am. Chem. Soc.*, 2024, DOI: **10.1021/jacs.4c01873**.
19 N. Kishi, Z. Li, K. Yoza, M. Akita and M. Yoshizawa, *J. Am. Chem. Soc.*, 2011, **133**, 11438–11441.
20 H. Nian, L. Cheng, L. Wang, H. Zhang, P. Wang, Y. Li and L. Cao, *Angew. Chem., Int. Ed.*, 2021, **60**, 15354–15358.
21 H. He, Y. J. Lee, Z. Zong, N. Liu, V. M. Lynch, J. Kim, J. Oh, D. Kim, J. L. Sessler and X.-S. Ke, *J. Am. Chem. Soc.*, 2023, **146**, 543–551.

22 Y. Shi, K. Cai, H. Xiao, Z. Liu, J. Zhou, D. Shen, Y. Qiu, Q.-H. Guo, C. Stern, M. R. Wasielewski, F. Diederich, W. A. Goddard and J. F. Stoddart, *J. Am. Chem. Soc.*, 2018, **140**, 13835–13842.
23 N. Kishi, M. Akita and M. Yoshizawa, *Angew. Chem., Int. Ed.*, 2014, **53**, 3604–3607.
24 J. Pfeuffer-Rooschüz, S. Heim, A. Prescimone and K. Tiefenbacher, *Angew. Chem., Int. Ed.*, 2022, **61**, e202209885.
25 S. E. Lewis, *Chem. Soc. Rev.*, 2015, **44**, 2221–2304.
26 I. Roy, A. H. G. David, P. J. Das, D. J. Pe and J. F. Stoddart, *Chem. Soc. Rev.*, 2022, **51**, 5557–5605.
27 R. Jasti, J. Bhattacharjee, J. B. Neaton and C. R. Bertozzi, *J. Am. Chem. Soc.*, 2008, **130**, 17646–17647.
28 H. Omachi, T. Nakayama, E. Takahashi, Y. Segawa and K. Itami, *Nat. Chem.*, 2013, **5**, 572–576.
29 P. Seitz, M. Bhosale, L. Rzesny, A. Uhlmann, J. S. Wössner, R. Wessling and B. Esser, *Angew. Chem., Int. Ed.*, 2023, **62**, e202306184.
30 J. C. Barnes, E. J. Dale, A. Prokofjevs, A. Narayanan, I. C. Gibbs-Hall, M. Juríček, C. L. Stern, A. A. Sarjeant, Y. Y. Botros, S. I. Stupp and J. F. Stoddart, *J. Am. Chem. Soc.*, 2015, **137**, 2392–2399.
31 V. G. Jiménez, A. H. G. David, J. M. Cuerva, V. Blanco and A. G. Campaña, *Angew. Chem., Int. Ed.*, 2020, **59**, 15124–15128.
32 P. Kumar, V. B. R. Mani Kandan, P. Balakrishnan, P. K. S. Antharjanam and V. Parthasarathy, *Angew. Chem., Int. Ed.*, 2023, **62**, e202305005.
33 S.-X. Fa, L.-X. Wang, D.-X. Wang, L. Zhao and M.-X. Wang, *J. Org. Chem.*, 2014, **79**, 3559–3571.
34 I. González-Veloso, J. Rodríguez-Otero and E. M. Cabaleiro-Lago, *Phys. Chem. Chem. Phys.*, 2016, **18**, 31670–31679.
35 B. Li, B. Wang, X. Huang, L. Dai, L. Cui, J. Li, X. Jia and C. Li, *Angew. Chem., Int. Ed.*, 2019, **58**, 3885–3889.
36 Z.-Y. Zhang and C. Li, *Acc. Chem. Res.*, 2022, **55**, 916–929.
37 H. Han, R. Fu, R. Wang, C. Tang, M.-M. He, J.-Y. Deng, D.-S. Guo, J. F. Stoddart and K. Cai, *J. Am. Chem. Soc.*, 2022, **144**, 20351–20362.
38 Y. Tian, Y. Guo, X. Dong, X. Wan, K.-H. Cheng, R. Chang, S. Li, X. Cao, Y.-T. Chan and A. C. H. Sue, *Nat. Synth.*, 2023, **2**, 395–402.
39 Y. F. Wang, H. Yao, L. P. Yang, M. Quan and W. Jiang, *Angew. Chem., Int. Ed.*, 2022, **61**, e202211853.
40 M. Yoshizawa and L. Catti, *Acc. Chem. Res.*, 2019, **52**, 2392–2404.
41 K. Hagiwara, Y. Sei, M. Akita and M. Yoshizawa, *Chem. Commun.*, 2012, **48**, 7678–7680.
42 K. Yazaki, M. Akita, S. Prusty, D. K. Chand, T. Kikuchi, H. Sato and M. Yoshizawa, *Nat. Commun.*, 2017, **8**, 15914.
43 K. Matsumoto, S. Kusaba, Y. Tanaka, Y. Sei, M. Akita, K. Aritani, M.-a. Haga and M. Yoshizawa, *Angew. Chem., Int. Ed.*, 2019, **58**, 8463–8467.
44 M. Yamashina, T. Yuki, Y. Sei, M. Akita and M. Yoshizawa, *Chem.–Eur. J.*, 2015, **21**, 4200–4204.
45 T. Lu and Q. Chen, *J. Comput. Chem.*, 2022, **43**, 539–555.
46 J.-D. Chai and M. Head-Gordon, *Phys. Chem. Chem. Phys.*, 2008, **10**, 6615–6620.
47 R. Krishnan, J. S. Binkley, R. Seeger and J. A. Pople, *J. Chem. Phys.*, 1980, **72**, 650–654.
48 T. Lu and F. Chen, *J. Comput. Chem.*, 2012, **33**, 580–592.